Supporting Information:

Characterization of μ-oxo-$(BsubPc)_2$ in Multiple Organic Photovoltaic Device Architectures: Comparing Against and Combining with Cl-BsubPc.

Jeffrey S. Castrucci,[†,‡,¶] *Richard K. Garner,* [†,¶] *Jeremy D. Dang,*[†] *Emmanuel Thibau,*[‡] *Zheng-Hong Lu,*[‡] *and Timothy P. Bender**[†,‡,§]

[†]Department of Chemical Engineering & Applied Chemistry, University of Toronto, Toronto, Ontario M5S 3E5, Canada

[‡]Department of Materials Science and Engineering, University of Toronto, 184 College Street, Toronto, Ontario M5S 3E4, Canada

[§]Department of Chemistry, University of Toronto, 80 St. George Street, Toronto, Ontario M5S 3H6, Canada

- to whom correspondences should be addressed. Email: tim.bender@utoronto.ca

¶ - these authors contributed equally to the preparation of this manuscript and the acquisition of the supporting experimental data.

Figure S1. Absorption spectrum (pink) of a 50 nm μ-oxo-$(BsubPc)_2$ film on a glass slide overlaid with the solar irradiance (gray = orbit, black = sea level) spectrum.

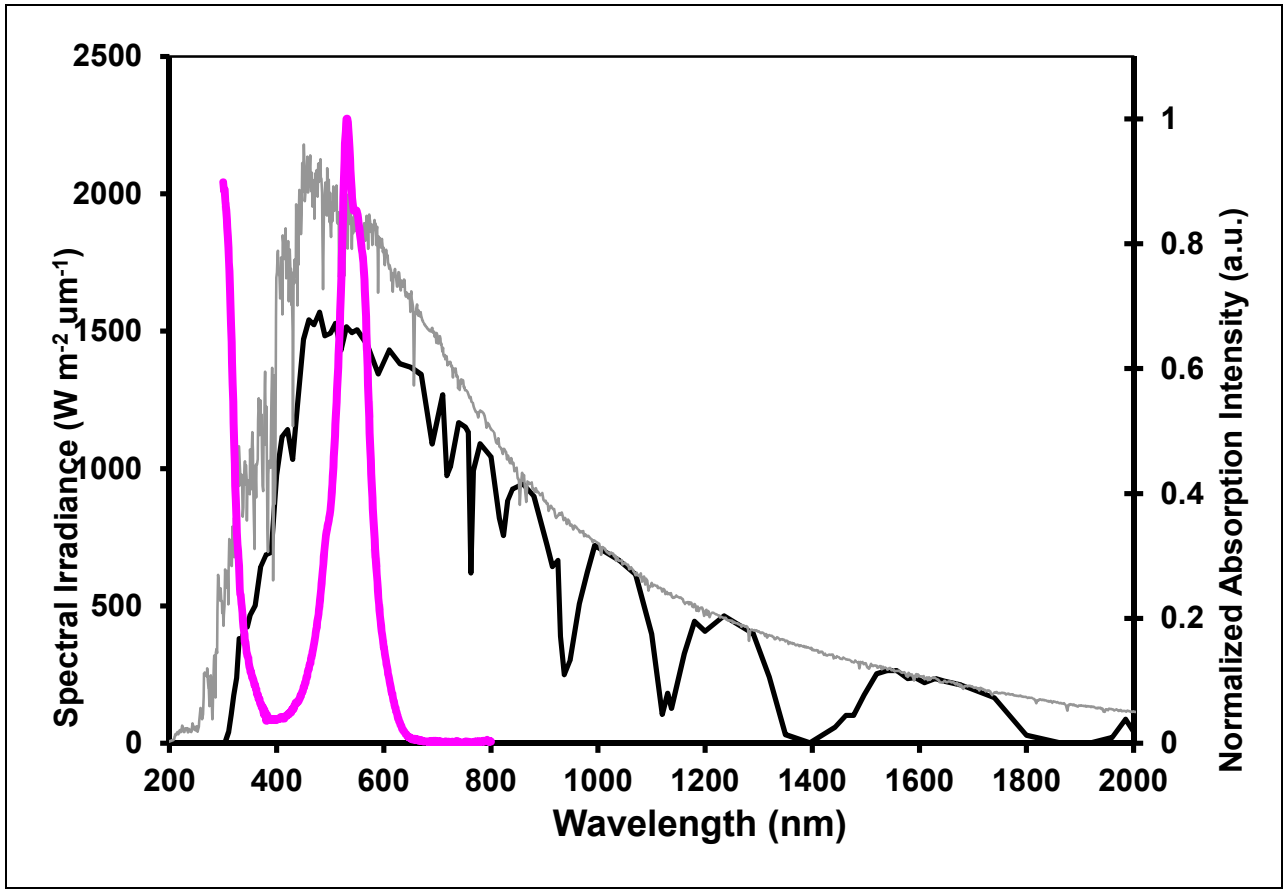

Figure S2. Ultraviolet photoelectron spectroscopy of a film of μ-oxo-$(BsubPc)_2$. (a) Identification of the HOMO to Fermi gap. (b) Identification of work function by way of secondary electron cut-off.

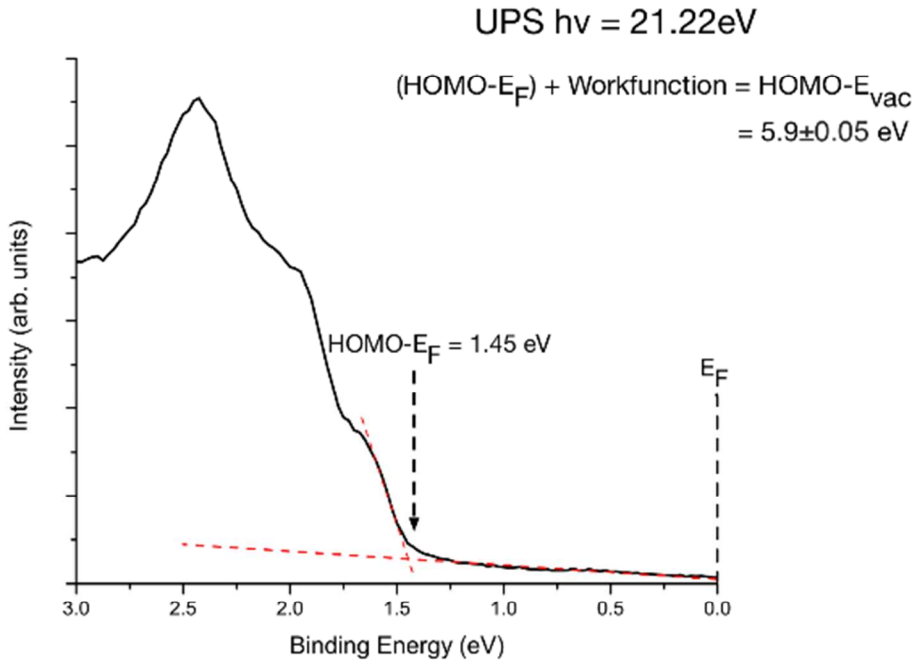

a)

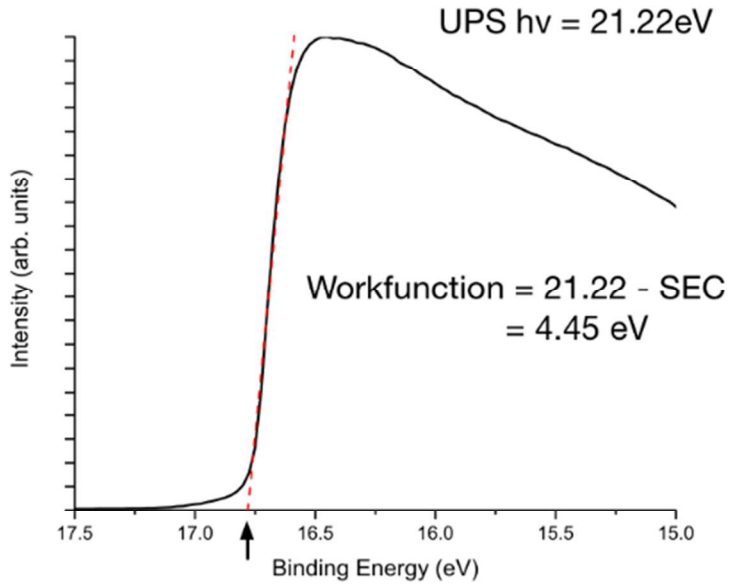

b)

Table S1. Material energy levels used to construct Figure 3. Work function, and HOMO and LUMO energy levels are reported relative to the vacuum level. LUMO energies are calculated as HOMO energy less the optical gap. Optical gap determined from absorption onset of 50 nm solid films of each material on glass slides.

Compound	**Work Function (eV)**	**E_{HOMO} (eV)**	**Optical Gap (eV)**	**E_{LUMO} (eV)**	**E_{HOMO} - Work Function (eV)**	**Work Function - E_{LUMO} (eV)**	**Source**
μ-oxo-$(BsubPc)_2$	4.5	5.9	1.9	4.0	1.4	0.5	This work
Cl-BsubPc	5.0	5.6	2.1	3.5	0.6	1.5	1
α6T	3.9	4.9	2.2	2.7	1.0	1.2	2
C_{60}	4.6	6.3	1.9	4.4	1.7	0.2	1
C_{70}	-	6.2	1.7	4.5	-	-	3
Cl-Cl_6BsubPc	-	5.9	2.1	3.8	-	-	4

Table S2. Mean device parameter comparison for reference devices containing TPBi electron transport layers and devices containing bathocuproine (BCP) electron transport layers (ETLs). Cascade and bilayer cells were tested. The standard deviation (SD) of each value is shown in parentheses. Device structure is ITO/PEDOT:PSS/MoO_x(5 nm)/Donor/C_{70}(30 nm)/ETL/Ag(80 nm).

Donor/d_D nm	**ETL/d_{ETL}**	**J_{SC} (SD)/ mA cm^{-2}**	**V_{OC} (SD)/V**	**FF (SD)**	**η_P (SD)/%**	**No. of cells tested**
Cl-BsubPc/10	BCP/10	4.1(0.13)	1.08(0.01)	0.51(0.02)	2.3(0.12)	20
Cl-BsubPc/10	TPBi/3	4.6(0.11)	1.08(0.01)	0.52(0.01)	2.6(0.09)	12
Cl-BsubPc/2.5, μ-oxo/7.5	BCP/10	5.7(0.08)	0.87(0.01)	0.61(0.01)	3.0(0.05)	14
Cl-BsubPc/2.5, μ-oxo/7.5	TPBi/3	5.9(0.17)	0.87(0.02)	0.64(0.02)	3.3(0.17)	14

Figure S3. JV curves for comparison of BCP ETL performance to TPBi ETL performance in bilayer and cascade devices. Shaded regions show the 95% confidence interval for the current flux. Device structure is ITO/PEDOT:PSS/MoO_x(5 nm)/Donor/C_{70}(30 nm)/ETL/Ag(80 nm).

Numerical data is tabulated in Table S2.

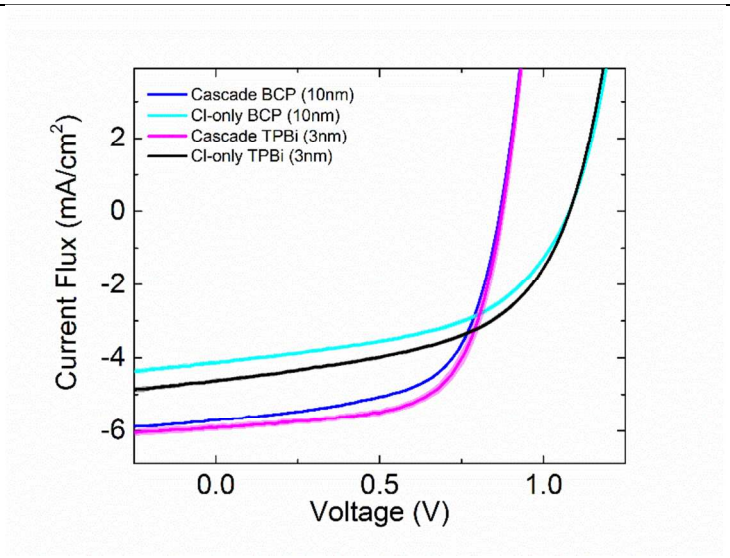

Table S3. Mean device parameter comparison for optimization of μ-oxo as an electron donor. The standard deviation (SD) of each value is shown in parentheses. Device structure is ITO/PEDOT:PSS/ Donor/Acceptor/TPBi(3 nm)/Ag(80 nm).

Donor/d_D nm	**Acceptor/d_A nm**	**J_{SC} (SD)/mA cm^{-2}**	**V_{OC} (SD)/V**	**FF (SD)**	**η_P (SD)/%**	**No. of cells tested**
μ-oxo/10	C_{60}/30	-3.6 (0.26)	0.80 (0.14)	0.36 (0.03)	1.0 (0.21)	12
μ-oxo/20	C_{60}/20	-2.3 (0.22)	0.70 (0.12)	0.27 (0.02)	0.43 (0.07)	12
μ-oxo/30	C_{60}/10	-1.2 (0.16)	0.45 (0.26)	0.25 (0.03)	0.13 (0.07)	12

Figure S4. JV curves for investigating of μ-oxo as an electron donor. Shaded regions show the 95% confidence interval for the current density. Device structure is ITO/PEDOT:PSS/ Donor/Acceptor/TPBi(3 nm)/Ag(80 nm). Numerical data is tabulated in Table S3.

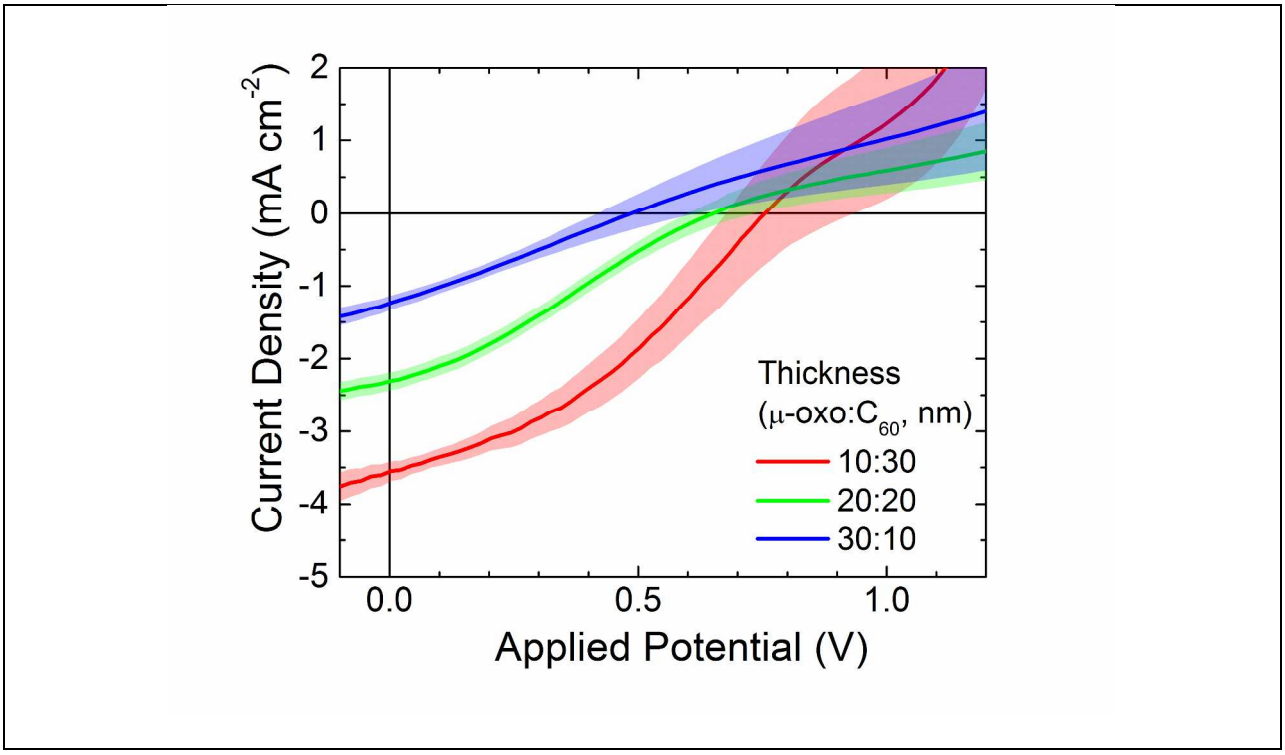

Table S4. Mean device parameter comparison for investigating μ-oxo as an electron donor with MoO_x hole extraction layer. The standard deviation (SD) of each value is shown in parentheses. Device structure is ITO/PEDOT:PSS/MoO_x/Donor/Acceptor/TPBi(3 nm)/Ag(80 nm).

Donor/d_D nm	**Acceptor/d_A nm**	**J_{SC} (SD)/mA cm^{-2}**	**V_{OC} (SD)/V**	**FF (SD)**	**η_P (SD)/%**	**No. of cells tested**
μ-oxo/5	C_{60}/30	-4.0 (0.15)	0.84 (0.02)	0.56 (0.06)	1.9 (0.27)	7
μ-oxo/8	C_{60}/45	-3.9 (0.13)	0.90 (0.003)	0.59 (0.01)	2.0 (0.07)	7
μ-oxo/10	C_{60}/60	-3.1 (0.13)	0.88 (0.07)	0.48 (0.36)	1.3 (0.20)	9

Figure S5. JV curves for optimization of μ-oxo as an electron donor with MoO_x hole extraction layer. Shaded regions show the 95% confidence interval for the current density. Device structure is ITO/PEDOT:PSS/MoO_x/Donor/Acceptor/TPBi(3 nm)/Ag(80 nm). Numerical data is tabulated in Table S4.

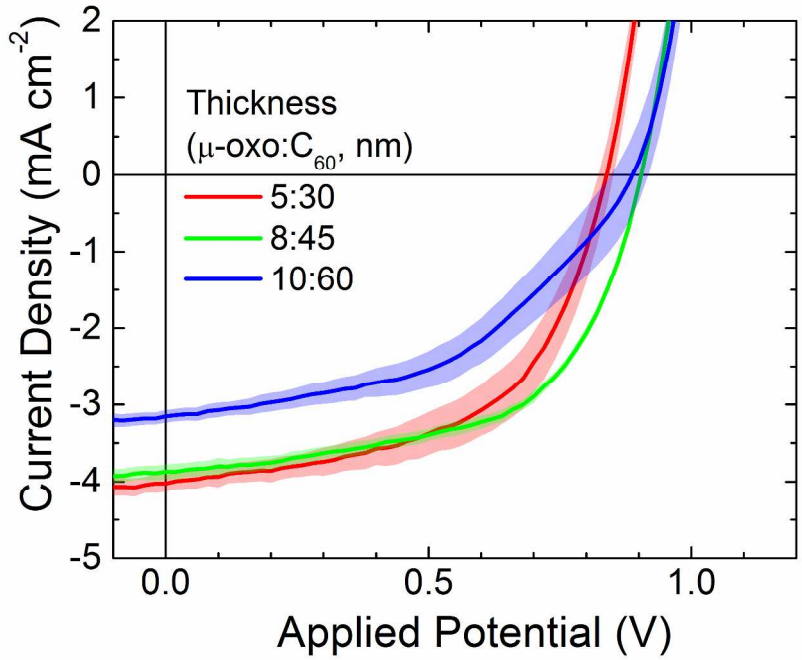

Table S5. Mean device parameter comparison for optimization of acceptor and donor layer thicknesses in μ-oxo/C70 devices. The standard deviation (SD) of each value is shown in parentheses. Device structure is ITO/PEDOT:PSS/MoO_x(5 nm)/Donor/Acceptor/TPBi(3 nm)/Ag(80 nm). The "5nm μ-oxo" device was fabricated with 5nm of TPBi instead of 3nm, leading to a drop in V_{OC}.

Donor/d_D nm	**Acceptor/d_A**	**J_{SC} (SD)/ mA cm^{-2}**	**V_{OC} (SD)/V**	**FF (SD)**	**η_P (SD)/%**	**No. of cells tested**
μ-oxo/5	C_{70}/30	5.8(0.06)	0.69(0.04)	0.55(0.01)	2.2(0.13)	14
μ-oxo/10	C_{70}/30	6.3(0.14)	0.91(0.01)	0.48(0.02)	2.7(0.15)	15
μ-oxo/16	C_{70}/30	5.3(0.03)	0.92(0.01)	0.41(0.01)	2.0(0.06)	10
μ-oxo/10	C_{70}/20	5.1(0.19)	0.91(0.01)	0.49(0.04)	2.3(0.11)	13
μ-oxo/10	C_{70}/30	6.3(0.14)	0.91(0.01)	0.48(0.02)	2.7(0.15)	15
μ-oxo/10	C_{70}/40	5.1(0.23)	0.90(0.01)	0.52(0.01)	2.4(0.16)	18

Figure S6. JV curves for optimization of donor and acceptor layer thicknesses in bilayer devices. Shaded regions show the 95% confidence interval for the current flux. Device structure is ITO/PEDOT:PSS/MoO_x(5 nm)/Donor/Acceptor/TPBi(3 nm)/Ag(80 nm). For varied C_{70} acceptor thickness, the donor layer is 10 nm of μ-oxo. For varied μ-oxo donor thickness, the acceptor layer is 30 nm of C_{70}. The "5nm μ-oxo" device was fabricated with 5nm of TPBi instead of 3nm, leading to a drop in V_{OC}. Numerical data is tabulated in Table S5.

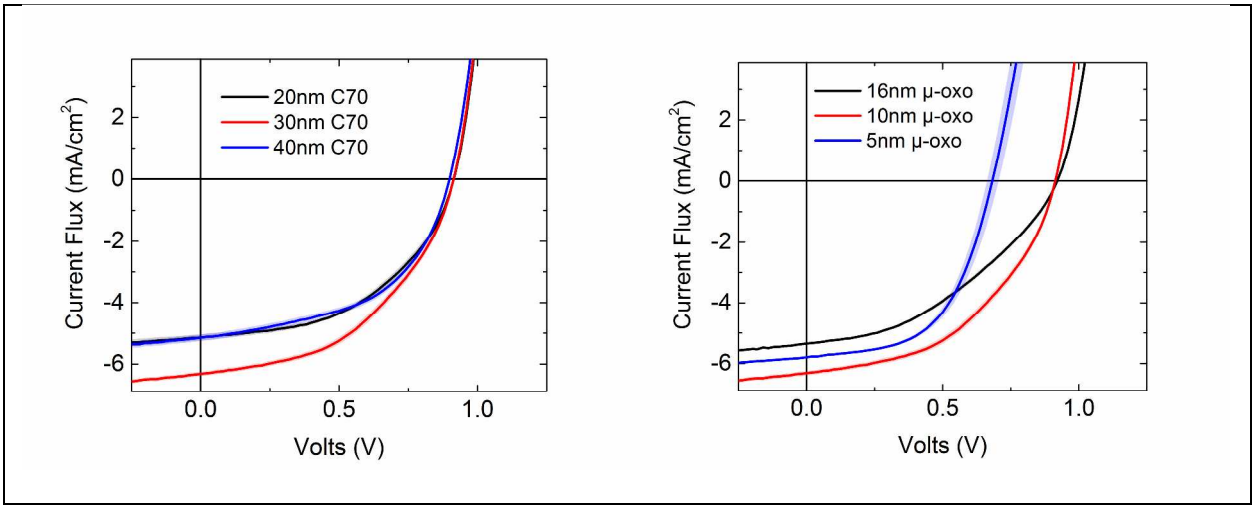

Table S6. Mean device parameter comparison for optimization of donor layer thicknesses in Cl-BsubPc/μ-oxo/C70 charge cascade devices. The standard deviation (SD) of each value is shown in parentheses. Device structure is ITO/PEDOT:PSS/MoO_x(5 nm)/Donors (10nm)/C_{70}(30 nm)/TPBi(3 nm)/Ag(80 nm).

Donor/d_D nm	**J_{SC} (SD)/mA cm^2**	**V_{OC} (SD)/V**	**FF (SD)**	**PCE (SD)/%**	**Cells Tested**
Cl-BsubPc/10	4.6(0.11)	1.08(0.01)	0.52(0.01)	2.6(0.09)	12
Cl-BsubPc/7.5, μ-oxo/2.5	5.6(0.04)	0.91(0.01)	0.60(0.01)	3.0(0.08)	16
Cl-BsubPc/5, μ-oxo/5	5.7(0.09)	0.89(0.01)	0.63(0.02)	3.2(0.14)	17
Cl-BsubPc/2.5, μ-oxo/7.5	5.9(0.17)	0.87(0.02)	0.64(0.02)	3.3(0.17)	14
μ-oxo-BsubPc/10	6.3(0.14)	0.91(0.01)	0.48(0.02)	2.7(0.15)	15

Figure S7. JV and EQE curves for optimization of Cl-BsubPc/μ-oxo/C70 cascade devices. Shaded regions show the 95% confidence interval for the current flux or external quantum efficiency. Device structure is ITO/PEDOT:PSS/MoO_x(5 nm)/Donors (10 nm)/C_{70}(30 nm)/TPBi(3 nm)/Ag(80 nm). Numerical data is tabulated in Table S6.

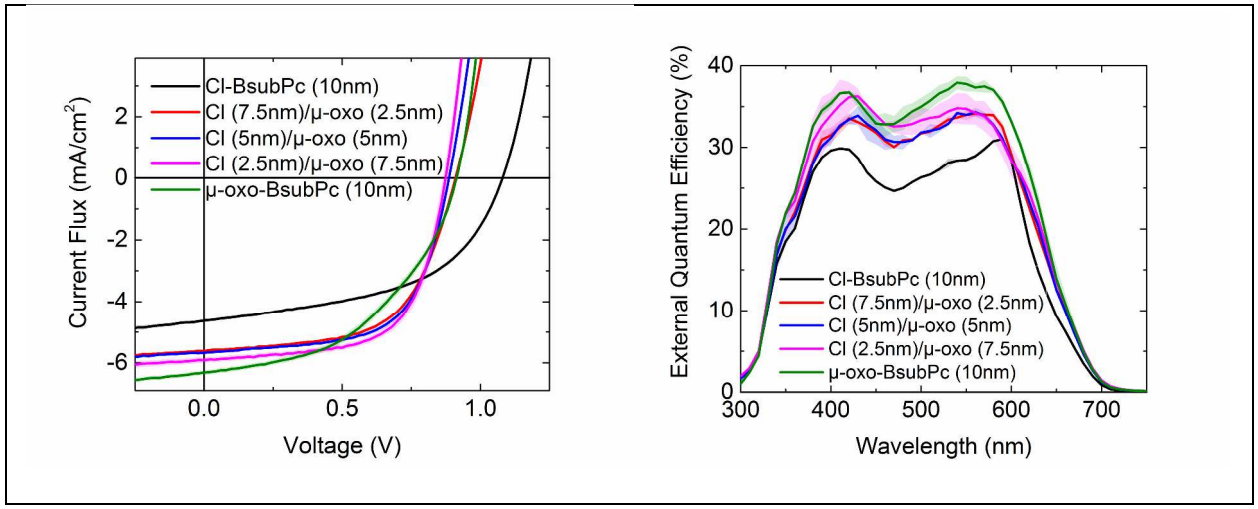

References

1. Morse, G. E.; Gantz, J. L.; Steirer, K. X.; Armstrong, N. R.; Bender, T. P. Pentafluorophenoxy Boron Subphthalocyanine (F_5BsubPc) as a Multifunctional Material for Organic Photovoltaics. *ACS Appl. Mater. Interfaces* **2014**, *6*, 1515-1524.

2. Ge, Y.; Whitten, J. E. Energy Level Alignment between Sexithiophene and Buckminsterfullerene Films. *Chem. Phys. Lett.* **2007**, *448*, 65-69.

3. Sakai, J.; Taima, T.; Yamanari, T.; Saito, K. Annealing Effect in the Sexithiophene:C_{70} Small Molecule Bulk Heterojunction Organic Photovoltaic Cells. *Sol. Energy Mater. Sol. Cells* **2009**, *93*, 1149-1153.

4. Castrucci, J. S.; Josey, D. S.; Thibau, E.; Lu, Z.-H.; Bender, T. P. Boron Subphthalocyanines as Triplet Harvesting Materials within Organic Photovoltaics. *J. Phys. Chem. Lett.* **2015,** *6* (15), 3121-3125.